J Electr Eng Technol.2018; 13(3): 1304-1316
http://doi.org/10.5370/JEET.2018.13.3.1304

ISSN(Print) 1975-0102
ISSN(Online) 2093-7423

Design and Implementation of an Adaptive Sliding-Mode Observer for Sensorless Vector Controlled Induction Machine Drives

Yanqing Zhang*, Zhonggang Yin†, Jing Liu* and Xiangqian Tong*

Abstract – An adaptive sliding-mode observer for speed estimation in sensorless vector controlled induction machine drives is proposed in this paper to balance the dilemma between the requirement of fast reaching transient and the chattering phenomenon reduction on the sliding-mode surface. It is well known that the sliding-mode observer (SMO) suffers from the chattering phenomenon. However, the reduction of the chattering phenomenon will lead to a slow transient process. In order to balance this dilemma, an adaptive exponential reaching law is introduced into SMO by optimizing the reaching way to the sliding-mode surface. The adaptive exponential reaching law is based on the options of an exponential term that adapts to the variations of the sliding-mode surface and system states. Moreover, the proposed sliding-mode observer considering adaptive exponential reaching law, which is called adaptive sliding-mode observer (ASMO), is capable for reducing the chattering phenomenon and decreasing the reaching time simultaneously. The stability analysis for ASMO is achieved based on Lyapunov stability theory. Simulation and experimental results both demonstrate the correctness and the effectiveness of the proposed method.

Keywords: Induction motor (IM), Sliding mode observer (SMO), Exponential reaching law, Speed estimation.

1. Introduction

Induction machine (IM) has many advantageous characteristics, such as high reliability, low cost and strong robustness compared with DC machines. The installation of speed sensors increases the cost and reduces the reliability and the robustness of IM drives. Hence, many attentions have been paid to rotor speed estimation to achieve speed sensorless control because of the merit of high reliability, low cost and disturbance rejection [1, 2]. A lot of sensorless methods have been proposed, such as low-frequency signal injection [3], high-frequency signal injection [4, 5], model reference adaptive systems (MRAS) [6, 7], adaptive full-order observers [8, 9], artificial neural network (ANN) [10], extended Kalman filters (EKF) [11, 12], and sliding-mode observers (SMO) [13-30].

In [3, 4], the estimation methods for rotor speed are based on low-frequency signal injection and high-frequency signal injection respectively, and they obtain good performance. With signal injections, the robustness of the speed estimation is strong, and the speed can be set at a very low level, even at zero. However, they are highly sophisticated and require customized designs for a particular IM drive, and there are estimated speed delays to the rotor speed due to the filter [5]. [6] presents a closed-loop model reference adaptive system (CL-MRAS), and a speed observer is developed for linear induction motor (LIM) drives. A new formulation of the reactive-power-based MRAS, which is stable in all four quadrants of operation, is proposed in [7]. However, in these researches, with respect to sensorless IM drives, the rotor flux and load torque should be known to realize the sensorless control. Moreover, these observers usually lose effectiveness or give inaccurate results due to the fact that their observability is poor in low speed region. In [8, 9], the robustness of the adaptive full-order observer against stator resistance and inductance variations is investigated, and the sesorless IM drives based on the proposed adaptive full-order observer can operate stable even in regenerating mode and in flux-weakening region. In [10], a new method based on ANNs applied to the parameter estimation of induction motors using sensorless vector control is proposed. Results obtained with this observer are more efficient than the results obtained with the classical observer. In [11, 12], a three-order EKF and an interfacing multiple-model EKF is used for speed and flux estimation in vector controlled induction motor drives, and experimental results have shown that the system based on EKF has good performance and applicable value.

Among the above rotor speed estimators, the sliding-mode observer (SMO) for speed estimation is popular and has been widely used because it has many merits such as simplicity of implementation, strong robustness to parameter deviations and disturbances rejection [13-16]. In recent years, SMO has been studied widely in the sensorless control of induction machines. In [17, 18], a sliding-mode current observer is proposed for rotor flux, rotor speed, and rotor time constant estimations. The rotor time constant update algorithm can overcome the problem

† Corresponding Author: Dept. of Electrical Engineering, Xi'an University of Technology, China. (zhgyin@xaut.edu.cn)
* Dept. of Electrical Engineering, Xi'an University of Technology, China. (zhangyanqing029@163.com, lstong@mail.xaut.edu.cn, jingliu@xaut.edu.cn)
Received: September 16, 2017; accepted: January 26, 2018

of rotor resistance variation, which is very important in indirect field-oriented vector control. In order to make the observer insensitive to the IM parameters, novel current model flux observers for speed sensorless control of IMs are proposed in [19, 20], by designing new structure of SMOs based on the dynamic model of IM, the proposed observers can work well over wide speed range and make the flux observer insensitive to the speed information or rotor resistance variation theoretically. In [21], two sliding-mode current observers are used to design an adaptive sliding-mode flux observer, which makes the observer robust to motor parameter variations. In [22], the sliding-mode observer has been applied to washing-machine drive applications, specifically, the proposed SMO focus on how to improve speed regulation, system robustness, and some special technical issues in washing-machine drives. By using a modified model of the induction motor in the rotating reference frame, an SMO for flux magnitude estimation is proposed in [23], with a certain gain selection, the proposed observer can be designed insensitive to the input speed inaccuracy.

On the other hand, based on characteristics of the sliding-mode observer, some novel sliding-mode theories or intelligent algorithms were introduced to build observers with new structures or higher performance. In [24, 25], a fractional order integral sliding-mode flux observer is proposed to take the advantage of the flexibility of fractional orders, in which the superiority is verified by numerical analyses, and the proposed observer can achieve better performance compared with conventional observer. To reduce the chattering problem caused by the classical SMO, a Fuzzy logic algorithm is introduced in [26] to replace the sign function. The robustness of proposed improved Fuzzy SMO in tracking application was verified at low and high speed and its hyper stability is guaranteed by Lyapunov criterion. In [27], the design of a scheme based on a discrete-time sliding mode observer which provides the rotor speed estimation is proposed, and the conditions for the existence of a discrete-time sliding switching hyper plane are analyzed. In [28], a new approach for sensorless vector control of IM using singularly perturbed sliding-mode observer is proposed, and the new approach is based on the singular perturbation theory which decomposes the original system of the observer error dynamics into separate slow and fast subsystems and permits a simple design and sequential determination of the observer gains. The new observer achieves good performance especially for the robustness against rotor resistance variation and external load disturbances.

It is well known that the sliding-mode observer (SMO) suffers from the chattering problem. However, the reduction of the chattering phenomenon will lead to a slow transient process. In previous studies, researches on the sliding-mode observer are focusing on the stability of the observer which ensures that the state variables can reach the sliding-mode surface in finite time. However, how the state variables reach the sliding-mode surface, i.e. the reaching way to the sliding-mode surface, has also the significant important influence on the performance of the observer, especially for the fast reaching transient performance and the chattering phenomenon reduction. Hence, to balance the dilemma between the requirement of fast reaching transient and the chattering phenomenon reduction on the sliding-mode surface, an adaptive exponential reaching law is introduced into SMO by optimizing the reaching way to the sliding-mode surface. The adaptive exponential reaching law is based on the options of an exponential term that adapts to the variations of the sliding-mode surface and system states. Besides, the proposed sliding-mode observer considering adaptive exponential reaching law, which is called adaptive sliding-mode observer (ASMO), is able to not only reducing the chattering phenomenon, but also decreasing the reaching time. Simulation and experimental results are presented to demonstrate the validity of the proposed approach.

2. IM Model and Sliding-Mode Observer Design for Sensorless IM Drives

2.1 Dynamic model of induction machine

With the stator currents and rotor fluxes defined as the state variables, the behaviour of IM in the stationary reference frame system can be modelled by continuous-time differential equations, and the IM model can be obtained in the matrix form as

$$\begin{bmatrix} \frac{di_{s\alpha}}{dt} \\ \frac{di_{s\beta}}{dt} \end{bmatrix} = k_1 \left(\begin{bmatrix} \lambda & \omega_r \\ -\omega_r & \lambda \end{bmatrix} \begin{bmatrix} \psi_{r\alpha} \\ \psi_{r\beta} \end{bmatrix} - \lambda L_m \begin{bmatrix} i_{s\alpha} \\ i_{s\beta} \end{bmatrix} \right) - k_2 \begin{bmatrix} i_{s\alpha} \\ i_{s\beta} \end{bmatrix} + k_3 \begin{bmatrix} u_{s\alpha} \\ u_{s\beta} \end{bmatrix} \tag{1}$$

$$\begin{bmatrix} \frac{d\psi_{r\alpha}}{dt} \\ \frac{d\psi_{r\beta}}{dt} \end{bmatrix} = -\left(\begin{bmatrix} \lambda & \omega_r \\ -\omega_r & \lambda \end{bmatrix} \begin{bmatrix} \psi_{r\alpha} \\ \psi_{r\beta} \end{bmatrix} - \lambda L_m \begin{bmatrix} i_{s\alpha} \\ i_{s\beta} \end{bmatrix} \right) \tag{2}$$

The constants k_1, k_2, k_3 and λ are defined as

$$k_1 = \frac{k_3 L_m}{L_r}, \quad k_2 = \frac{R_s}{\sigma L_s}, \quad k_3 = \frac{1}{\sigma L_s}, \quad \lambda = \frac{R_r}{L_r}.$$

In addition, a new matrix G is defined as

$$G = \left(\begin{bmatrix} \lambda & \omega_r \\ -\omega_r & \lambda \end{bmatrix} \begin{bmatrix} \psi_{r\alpha} \\ \psi_{r\beta} \end{bmatrix} - \lambda L_m \begin{bmatrix} i_{s\alpha} \\ i_{s\beta} \end{bmatrix} \right) \tag{3}$$

2.2 Preliminaries of sliding-mode observer

It is noted from (1) and (2) that the matrix G appears as a

common term both in the current equation and in the flux linkage equation. Thus it can be concluded that the advantage of (1) and (2) is that the coupling terms between α and β axes are exactly the same, which means that the coupling terms can be replaced with the same sliding-mode function. Therefore, the estimation of the matrix G can be provided by the sliding-mode function, which can be described as

$$\begin{bmatrix} f_\alpha \\ f_\beta \end{bmatrix} = \hat{G} = \begin{bmatrix} \lambda & \hat{\omega}_r \\ -\hat{\omega}_r & \lambda \end{bmatrix} \begin{bmatrix} \hat{\psi}_{r\alpha} \\ \hat{\psi}_{r\beta} \end{bmatrix} - \lambda L_m \begin{bmatrix} \hat{i}_{s\alpha} \\ \hat{i}_{s\beta} \end{bmatrix} \tag{4}$$

Hence, based on (1), the sliding-mode observer for current observation is transformed into

$$\begin{bmatrix} \frac{d\hat{i}_{s\alpha}}{dt} \\ \frac{d\hat{i}_{s\beta}}{dt} \end{bmatrix} = k_1 \begin{bmatrix} f_\alpha \\ f_\beta \end{bmatrix} - k_2 \begin{bmatrix} \hat{i}_{s\alpha} \\ \hat{i}_{s\beta} \end{bmatrix} + k_3 \begin{bmatrix} u_{s\alpha} \\ u_{s\beta} \end{bmatrix} \tag{5}$$

Simultaneously, based on (2), the sliding-mode observer for flux observation can be presented as

$$\begin{bmatrix} \frac{d\hat{\psi}_{r\alpha}}{dt} \\ \frac{d\hat{\psi}_{r\beta}}{dt} \end{bmatrix} = - \begin{bmatrix} f_\alpha \\ f_\beta \end{bmatrix} \tag{6}$$

where

$$\begin{bmatrix} f_\alpha \\ f_\beta \end{bmatrix} = - \begin{bmatrix} \lambda_0 sign(S_\alpha) \\ \lambda_0 sign(S_\beta) \end{bmatrix} \tag{7}$$

and $\lambda_0 > 0$,

$$\begin{bmatrix} S_\alpha \\ S_\beta \end{bmatrix} = \begin{bmatrix} \tilde{i}_{s\alpha} \\ \tilde{i}_{s\beta} \end{bmatrix} = \begin{bmatrix} \hat{i}_{s\alpha} - i_{s\alpha} \\ \hat{i}_{s\beta} - i_{s\beta} \end{bmatrix} \tag{8}$$

Conventionally, the sliding-mode surface is defined by considering the estimated error of stator currents

$$S = \begin{bmatrix} S_\alpha & S_\beta \end{bmatrix}^T \tag{9}$$

In this paper, the sliding-mode surface is defined by considering the estimated error of stator currents and the rate of the estimated error simultaneously. For the purpose of improving the accuracy of control performance, the new sliding-mode surface is shown as

$$S_I = \begin{bmatrix} S_{I\alpha} \\ S_{I\beta} \end{bmatrix} = \begin{bmatrix} p_1 \tilde{i}_{s\alpha} + p_2 \int \tilde{i}_{s\alpha} dt \\ p_1 \tilde{i}_{s\beta} + p_2 \int \tilde{i}_{s\beta} dt \end{bmatrix} \tag{10}$$

where $p_1 > 0$ and $p_2 > 0$. The parameters p_1 and p_2 are the adjustable parameters which are used to regulate the proportion of the estimated error and the rate of the estimated error. In practical application, the value of p_1 should be designed smaller than p_2 since a large value of p_1 will aggravate the chattering phenomenon.

Traditionally, the sliding-mode surface without considering the rate of the estimated error can not guarantee the robustness during the reaching phase, i.e. before sliding-mode occurs. In this paper, for the sliding-mode surface defined by considering the estimated error and the rate of the estimated error simultaneously, the system trajectories can be established without a reaching phase, and the concept of the rate of estimated error concentrates on the robustness of the motion in the whole state space, i.e. the robustness of the system can be guaranteed throughout an entire response of the system starting from the initial time instance.

3. Adaptive Sliding-Mode Observer Design for Sensorless IM Drives

It is well known that the sliding-mode observer (SMO) suffers from the chattering problem. However, the reduction of the chattering phenomenon will leads to a slow transient process. In previous studies, researches on the sliding-mode observer are focusing on the stability of the observer which ensures that the state variables can reach the sliding-mode surface in finite time. However, the reaching way to the sliding-mode surface is rarely concerned. In fact, the reaching way to the sliding-mode surface has significant important influence on the performance of SMO, especially for the fast reaching transient performance and the chattering phenomenon reduction. Hence, to optimize the observation performance of SMO, the reaching law method is introduced in this paper to help designing the sliding-mode observer.

3.1 Design of the sliding-mode observer considering conventional exponential reaching law

In order to optimize the observation performance of sliding mode observer, a typical reaching law called exponential reaching law is introduced into SMO by considering the reaching way to the sliding-mode surface.

From (2)-(6) and (10), the derivative of S_I can be derived as

$$\begin{aligned} \dot{S}_I &= p_1 \begin{bmatrix} \dot{\hat{i}}_{s\alpha} - \dot{i}_{s\alpha} \\ \dot{\hat{i}}_{s\beta} - \dot{i}_{s\beta} \end{bmatrix} + p_2 \begin{bmatrix} \tilde{i}_{s\alpha} \\ \tilde{i}_{s\beta} \end{bmatrix} \\ &= -p_1 k_1 \begin{bmatrix} M \\ N \end{bmatrix} + (p_2 - p_1 k_2) \begin{bmatrix} \tilde{i}_{s\alpha} \\ \tilde{i}_{s\beta} \end{bmatrix} + p_1 k_1 \begin{bmatrix} \frac{d\hat{\psi}_{r\alpha}}{dt} \\ \frac{d\hat{\psi}_{r\beta}}{dt} \end{bmatrix} \end{aligned} \tag{11}$$

where

$$M = -\lambda\psi_{r\alpha} - \omega_r\psi_{r\beta} + \lambda L_m i_{s\alpha},$$
$$N = \omega_r\psi_{r\alpha} - \lambda\psi_{r\beta} + \lambda L_m i_{s\beta}.$$

The reaching law method is introduced to optimize the speed observation performance of SMO, and for the specific reaching law, the exponential reaching law is adopted as follows

$$\dot{S}_I = -k \cdot sign(S_I) - \mu \cdot S_I = -k\begin{bmatrix} sign(S_{I\alpha}) \\ sign(S_{I\beta}) \end{bmatrix} - \mu\begin{bmatrix} S_{I\alpha} \\ S_{I\beta} \end{bmatrix} \quad (12)$$

where $k > 0$ and $\mu > 0$.

Based on (11) and (12), the relationship between sliding-mode flux observer and the exponential reaching law can be derived as follows

$$\begin{aligned} &-p_1k_1\begin{bmatrix} M \\ N \end{bmatrix} + (p_2 - p_1k_2)\begin{bmatrix} \tilde{i}_{s\alpha} \\ \tilde{i}_{s\beta} \end{bmatrix} + p_1k_1\begin{bmatrix} \dfrac{d\hat{\psi}_{r\alpha}}{dt} \\ \dfrac{d\hat{\psi}_{r\beta}}{dt} \end{bmatrix} \\ &= -k\begin{bmatrix} sign(S_{I\alpha}) \\ sign(S_{I\beta}) \end{bmatrix} - \mu\begin{bmatrix} S_{I\alpha} \\ S_{I\beta} \end{bmatrix} \end{aligned} \quad (13)$$

From (13), the rotor flux in SMO can be observed as follows

$$\begin{aligned} \begin{bmatrix} \dfrac{d\hat{\psi}_{r\alpha}}{dt} \\ \dfrac{d\hat{\psi}_{r\beta}}{dt} \end{bmatrix} &= -\begin{bmatrix} f'_\alpha \\ f'_\beta \end{bmatrix} - \frac{k}{p_1k_1}\begin{bmatrix} sign(S_{I\alpha}) \\ sign(S_{I\beta}) \end{bmatrix} \\ &\quad - \frac{p_2 - p_1k_2 + p_1\mu}{p_1k_1}\begin{bmatrix} \tilde{i}_{s\alpha} \\ \tilde{i}_{s\beta} \end{bmatrix} - \frac{\mu p_2}{p_1k_1}\begin{bmatrix} \int \tilde{i}_{s\alpha}dt \\ \int \tilde{i}_{s\beta}dt \end{bmatrix} \end{aligned} \quad (14)$$

where the sliding-mode function can be written as

$$\begin{bmatrix} f'_\alpha \\ f'_\beta \end{bmatrix} = -\begin{bmatrix} \lambda_0 sign(S_{I\alpha}) \\ \lambda_0 sign(S_{I\beta}) \end{bmatrix} \quad (15)$$

With the current observer shown in (5), the sliding-mode observer with exponential reaching law is constructed by considering the reaching way to the sliding-mode surface.

For the sliding-mode observer considering conventional exponential reaching law, the dynamic performance is directly related to the value of k and μ. By integrating (12) with respect to time, the time required to reach sliding-mode surface can be derived as

$$\left|\int_0^t \dot{S}_I dt\right| = \left|\int_0^t k dt\right| + \left|\int_0^t (\mu \cdot S_I)dt\right| \quad (16)$$

Based on (12) and (16), the required time can be derived as

$$t = \frac{|S_I(t) - S_I(0)| - \left|\int_0^t (\mu \cdot S_I)dt\right|}{k} \quad (17)$$

It is obvious that $S_I(t)=0$ based on the sliding-mode control theory, thus (17) can be rewritten as follows

$$t = \frac{|S_I(0)| - \left|\int_0^t (\mu \cdot S_I)dt\right|}{k} \quad (18)$$

It is noted from (18) that the reaching time t can be reduced by setting high values of k and μ. However, the high values of k and μ will directly increase the chattering level because of the sliding-mode inherent characteristic. To further improve the performance of SMO, i.e. to further optimize the reaching way to the sliding mode surface, an adaptive exponential reaching law is introduced into sliding-mode observer for speed estimation in sensorless IM drives.

3.2 Design of the sliding-mode observer considering adaptive exponential reaching law

The proposed adaptive sliding-mode observer (ASMO) is considering an adaptive exponential reaching law, and in which the adaptive exponential reaching law is realized based on the option of an exponential term that adapts to the variations of the system states and the sliding-mode surface. This adaptive exponential reaching law is the optimization of (12) which is given by

$$\begin{cases} \dot{S}_I = -g(\tilde{i}_s) \cdot sign(S_I) - \mu \cdot S_I \\ g(\tilde{i}_s) = \dfrac{k'}{\varepsilon + (1 + 1/|\tilde{i}_s| - \varepsilon)e^{-\eta|\delta|}} \end{cases} \quad (19)$$

where $k' > 0$, $\eta > 0$, $0 < \varepsilon < 1$ and $\delta = \hat{i}_{s\alpha}i_{s\beta} - i_{s\alpha}\hat{i}_{s\beta}$.

It is noted from this adaptive exponential reaching law that if the state variables are far away from the sliding-mode surface, which means that $|\delta|$ increases, then the equation $g(\tilde{i}_s)$ converges to k'/ε. Thus a faster reaching time is obtained since $k'/\varepsilon > k'$. In addition, if the state variables is close to the sliding-mode surface, which means that $|\delta|$ decreases, the denominator term of the equation $g(\tilde{i}_s)$ becomes $1 + 1/|\tilde{i}_s|$, then $g(\tilde{i}_s)$ converges to $k'|\tilde{i}_s|/(1 + |\tilde{i}_s|)$, in which $\tilde{i}_s$ gradually decreases to zero. This indicates that $g(\tilde{i}_s)$ can suppress the chattering problem by decreasing to zero gradually when the state variable is close to the sliding-mode surface. Therefore, the

proposed ASMO can overcome the variations of the sliding-mode surface and system states dynamically since $0 < g(\tilde{i}_s) < k'/\varepsilon$.

Based on (14) and (19), the rotor flux in ASMO can be observed as follows

$$\begin{bmatrix} \frac{d\hat{\psi}_{r\alpha}}{dt} \\ \frac{d\hat{\psi}_{r\beta}}{dt} \end{bmatrix} = -\begin{bmatrix} f'_\alpha \\ f'_\beta \end{bmatrix} - \frac{g(\tilde{i}_s)}{p_1 k_1}\begin{bmatrix} sign(S_{I\alpha}) \\ sign(S_{I\beta}) \end{bmatrix} - \frac{p_2 - p_1 k_2 + p_1 \mu}{p_1 k_1}\begin{bmatrix} \tilde{i}_{s\alpha} \\ \tilde{i}_{s\beta} \end{bmatrix} - \frac{\mu p_2}{p_1 k_1}\begin{bmatrix} \int \tilde{i}_{s\alpha} dt \\ \int \tilde{i}_{s\beta} dt \end{bmatrix} \tag{20}$$

With the current observer shown in (5), the proposed ASMO has been established, and the stability analysis for the proposed observer is presented in the Appendices.

For the proposed adaptive sliding-mode observer, the decrease of the reaching time and the reduction of the chattering phenomenon can be satisfied simultaneously. According to (19), the reaching time t_1 that is the required time for system states to reach the sliding-mode surface can be calculated as

$$(\dot{S}_I + \mu \cdot S_I)\left[\varepsilon + (1 + 1/|x_1| - \varepsilon)e^{-\eta|\delta|}\right] = -k' \cdot sign(S_I) \tag{21}$$

With $S_I(t)$=0, integrating (21) from 0 to t_1 will yield

$$t_1 = \frac{(1 + 1/|x_1| - \varepsilon)[\int_0^{t_1} e^{-\eta|\delta|}dt + \mu\int_0^{t_1} e^{-\eta|\delta|}dt] - \varepsilon S_I(0) + \mu\varepsilon\int_0^{t_1} S_I dt}{-k'} \tag{22}$$

Since $1 - e^{-\eta|S_I(0)|} < 1$, and the parameter η can be chosen such that $\eta >> 1 + 1/|x_1| - \varepsilon$, then (22) can be simplified as

$$t_1 < \frac{1}{k'}(\varepsilon|S_I(0)| + \mu\varepsilon\left|\int_0^{t_1} S_I dt\right|) \tag{23}$$

It can be seen from (23) that parameter η has no influence on the reaching time of the adaptive exponential reaching law, and the smaller the value of ε is, the shorter the reaching time will be. Therefore, in order to achieve a faster tracking performance of observer, a smaller value of ε should be chosen.

Then substituting $t_1 = t + \Delta t$ into inequality (23) yields

$$t_1 < \frac{1}{k'}(\varepsilon|S_I(0)| - \varepsilon\left|\int_0^t \mu S_I dt + \int_t^{t+\Delta t} \mu S_I dt\right|) \tag{24}$$

where t is the reaching time of the conventional exponential reaching law and Δt is the time difference between the conventional exponential reaching law and the adaptive exponential reaching law. Noticing that the flowing inequality (25) is always correct

$$\left|\int_0^t \mu S_I dt + \int_t^{t+\Delta t} \mu S_I dt\right| < \left|\int_0^t \mu S_I dt\right| + \left|\int_t^{t+\Delta t} \mu S_I dt\right| \tag{25}$$

Then the inequality (26) can be obtained

$$t_1 < \frac{1}{k'}\left[\varepsilon|S_I(0)| - \varepsilon\left(\left|\int_0^t \mu S_I dt\right| + \left|\int_t^{t+\Delta t} \mu S_I dt\right|\right)\right] \tag{26}$$

Therefore, according to (20) and (26), the time difference between t_1 and t can be derived as follows if $k = k'$

$$\begin{aligned} t - t_1 &> \frac{|S_I(0)| - \left|\int_0^t \mu S_I dt\right|}{k} - \frac{\varepsilon|S_I(0)| - \varepsilon\left|\int_0^t \mu S_I dt\right| - \varepsilon\left|\int_t^{t+\Delta t} \mu S_I dt\right|}{k'} \\ &= \frac{|S_I(0)| - \left|\int_0^t \mu S_I dt\right|}{k}(1 - \varepsilon) + \frac{\varepsilon\left|\int_t^{t+\Delta t} \mu S_I dt\right|}{k} \end{aligned} \tag{27}$$

It is noted from (27) that $1 - \varepsilon > 0$ since $k' > 0$ and $0 < \varepsilon < 1$, then (27) indicates that t - $t_1 > 0$. This indicates that the proposed adaptive exponential reaching law has a faster reaching speed when $k = k'$. In addition, if the reaching times of the two reaching law are equal (i.e. $t = t_1$ and Δt = 0), then the following expression can be derived as

$$k' = \varepsilon k \tag{28}$$

Hence, it can be concluded that $k' < k$ since $0 < \varepsilon < 1$, which means that by using the proposed adaptive exponential reaching law, the chattering phenomenon of SMO can be reduced with the same reaching speed.

3.3 Speed estimation of IM based on adaptive sliding-mode observer

According to (20), the rotor flux linkage can be calculated without knowing the information of the rotor speed, thus the system will be implemented simply. Moreover, the rotor speed can be obtained based on the above observed fluxes. From (15) and (20), the information of estimated speed can be obtained as

$$\begin{bmatrix} f'_\alpha \\ f'_\beta \end{bmatrix} = \left(\begin{bmatrix} \lambda & \hat{\omega}_r \\ -\hat{\omega}_r & \lambda \end{bmatrix}\begin{bmatrix} \hat{\psi}_{r\alpha} \\ \hat{\psi}_{r\beta} \end{bmatrix} - \lambda L_m \begin{bmatrix} \hat{i}_{s\alpha} \\ \hat{i}_{s\beta} \end{bmatrix}\right) \tag{29}$$

By multiplying row one by $\hat{\psi}_{r\beta}$ and row two by $\hat{\psi}_{r\alpha}$, then (29) can be rewritten as

$$\begin{bmatrix} \hat{\psi}_{r\beta} f'_\alpha \\ \hat{\psi}_{r\alpha} f'_\beta \end{bmatrix} = \left(\begin{bmatrix} \hat{\psi}_{r\beta}\lambda & \hat{\psi}_{r\beta}\hat{\omega}_r \\ -\hat{\psi}_{r\alpha}\hat{\omega}_r & \hat{\psi}_{r\alpha}\lambda \end{bmatrix}\begin{bmatrix} \hat{\psi}_{r\alpha} \\ \hat{\psi}_{r\beta} \end{bmatrix} - \lambda L_m \begin{bmatrix} \hat{\psi}_{r\beta}\hat{i}_{s\alpha} \\ \hat{\psi}_{r\alpha}\hat{i}_{s\beta} \end{bmatrix}\right) \tag{30}$$

Then the row one and row two in (30) can be derived as

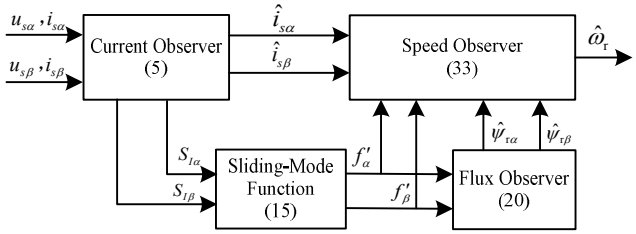

Fig. 1. The structure of adaptive sliding-mode observer (ASMO)

$$\hat{\psi}_{r\beta} f'_{\alpha} = \hat{\psi}_{r\alpha}\hat{\psi}_{r\beta}\lambda + \hat{\psi}^2_{r\beta}\hat{\omega}_r - \lambda L_m \hat{\psi}_{r\beta}\hat{i}_{s\alpha} \tag{31}$$

$$\hat{\psi}_{r\alpha} f'_{\beta} = \hat{\psi}_{r\alpha}\hat{\psi}_{r\beta}\lambda - \hat{\psi}^2_{r\alpha}\hat{\omega}_r - \lambda L_m \hat{\psi}_{r\alpha}\hat{i}_{s\beta} \tag{32}$$

Based on (31) and (32), the estimated speed $\hat{\omega}_r$ can be calculated as

$$\hat{\omega}_r = \frac{\hat{\psi}_{r\beta} f'_{\alpha} - \hat{\psi}_{r\alpha} f'_{\beta} - \lambda L_m (\hat{i}_{s\beta}\hat{\psi}_{r\alpha} - \hat{i}_{s\alpha}\hat{\psi}_{r\beta})}{\hat{\psi}^2_{r\alpha} + \hat{\psi}^2_{r\beta}} \tag{33}$$

The structure of overall adaptive sliding-mode observer along with the speed estimator is shown in Fig. 1. When the estimation error trajectories reach the sliding surface, i.e. S_I=[0 0]^T, then the observed error between the actual currents and estimated currents will converge to zero, and the observed rotor flux will be forced to converge to the real rotor flux simultaneously.

4. IM Speed Estimation Method Based on Adaptive Sliding-mode Observer

It is the essence of the sensorless vector control that the rotor speed is not acquired by mechanical sensor, but rather by software in speed regulating system. The block diagram of the sensorless IM drive based on the adaptive sliding-mode observer is shown in Fig. 2. As shown, the phase currents and the voltages of the IM are transformed to α-β coordinate system. Since the purpose of the drive system is to obtain a sensorless design, the rotor speed is estimated by the observer and fed back to PI regulator.

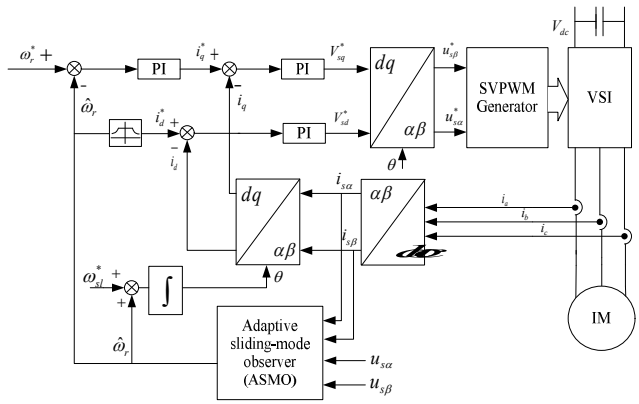

Fig. 2. Block diagram of the control system based on adaptive sliding-mode observer (ASMO)

5. Simulation Results

In order to validate the theoretical analysis and to verify the performance of the proposed approach, the simulation is carried out by MATLAB/Simulink. The parameters of the tested induction machine are listed in Table 1.

Table 1. IM parameters

P_N	1.1 kW	R_s	5.27 Ω
U_N	380 V	R_r	5.07 Ω
I_N	2.9 A	L_m	0.421 H
f_N	50 Hz	L_s	0.423 H
n_N	1410 rpm	L_r	0.479 H
T_N	7.45 N · m	P	2

The simulations are presented by setting different speed commands ω_r^*, 15 rpm, 500 rpm, 1000 rpm and 1500 rpm, including the whole speed range. Moreover, the simulation results are provided by calculating the estimation errors between the real speed ω_r and the estimated speed $\hat{\omega}_r$. As can be seen in Fig. 3, ω_r^* is set as follows: the initial ω_r^* is set as 0, and then ω_r^* is set at 15 rpm at 0.1 s, 500 rpm at 1.5 s, 1000 rpm at 3 s and 1500 rpm at 4.5 s, respectively. It can be seen that both SMO and ASMO have good tracking performance, and in which the estimation error of SMO is larger than ASMO. In addition, the induction machine is running without load disturbance in the beginning, and at 6 s, a step rated load is added suddenly. It is known that the sliding-mode surface in SMO is built based on the estimated current error and the rate of the estimated current error, and thus the waveforms of the sliding-mode surface are oscillating near zero since the amplitude of actual stator currents of IM are constantly changing. When the step rated load is added, the oscillation of the sliding-mode surface is aggravated because the stator current is changing suddenly, and then the estimated current tracks the actual current and the waveforms of the sliding-mode surface keeps stable after loading. It can been seen that the proposed ASMO can provide better steady property and also has faster reaching time compared to the conventional SMO.

Fig. 4 presents the rotor speed response when IM runs from forward to reverse. The setting speed ω_r^* is set as follows: the initial ω_r^* is set as 0, and then ω_r^* is set at 1500 rpm at 0.1 s, -1500 rpm at 2 s and 0 at 4 s, respectively. As can be seen in Fig. 4, both SMO and ASMO have good tracking performance, and the drive system keeps stable when the IM runs from forward to reverse. In addition, the ASMO can present better speed estimation accuracy both in steady state and in transient process.

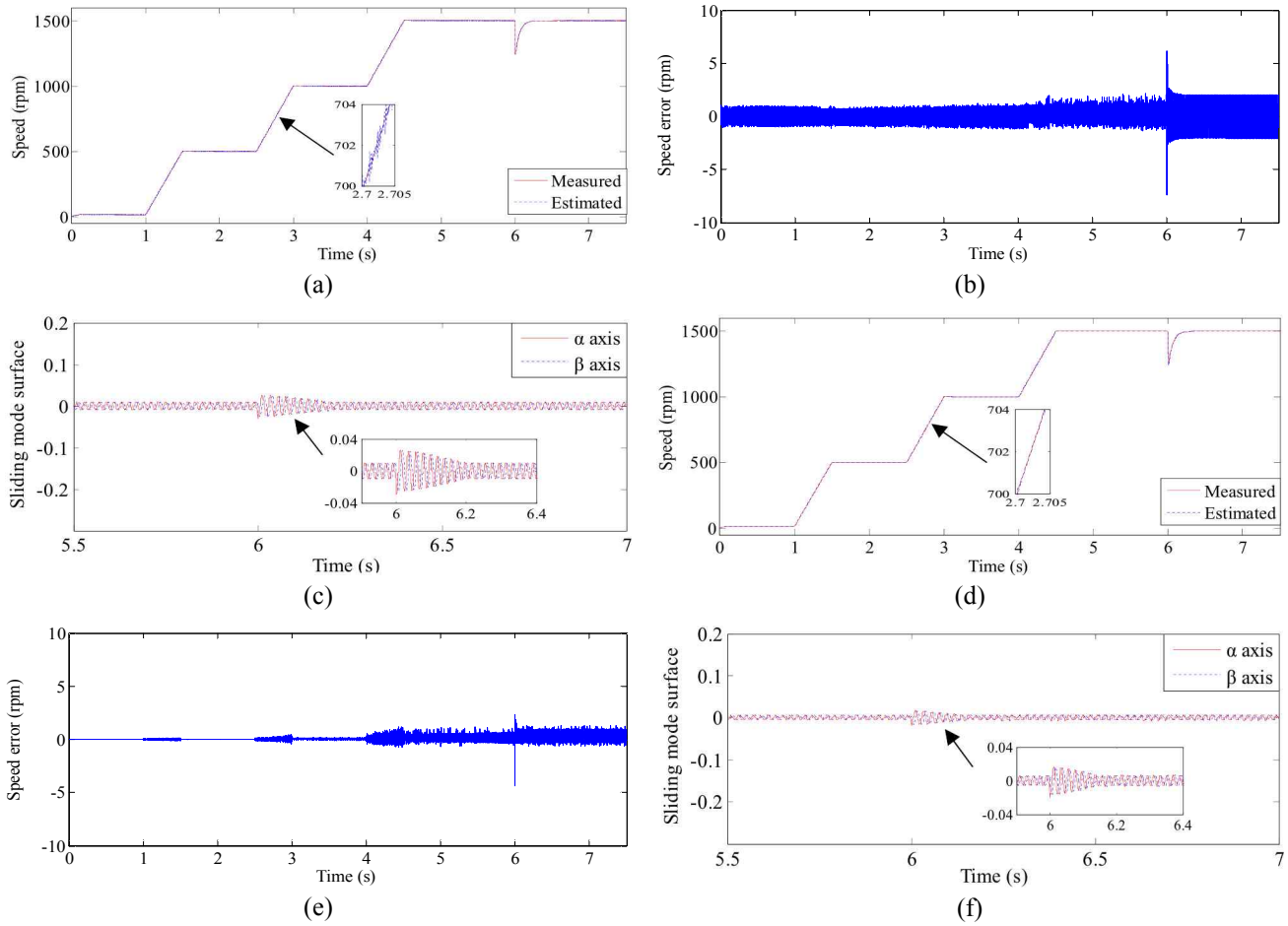

Fig. 3. Simulation results with different speed commands. (a) Speed response based on SMO. (b) Speed error based on SMO. (c) Waveforms of the sliding-mode surface based on SMO. (d) Speed response based on ASMO. (e) Speed error based on ASMO. (f) Waveforms of the sliding-mode surface based on ASMO

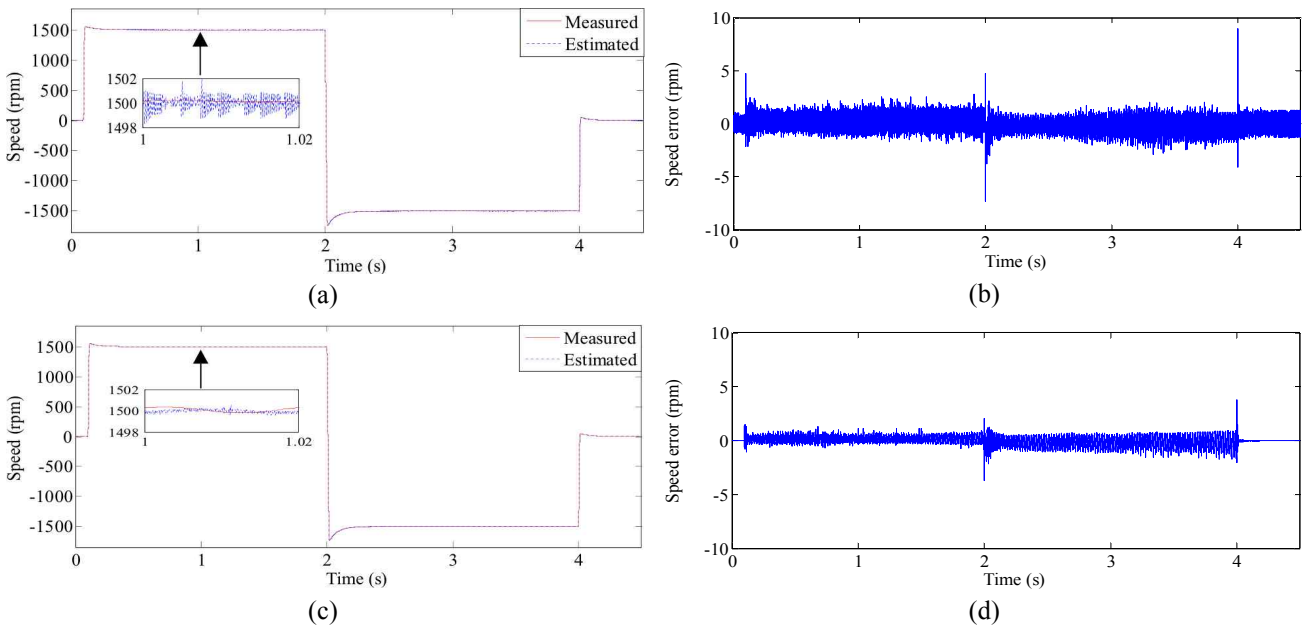

Fig. 4. Simulation results when the IM runs from forward to reverse. (a) Speed response based on SMO. (b) Speed error based on SMO. (c) Speed response based on ASMO. (d) Speed error based on ASMO

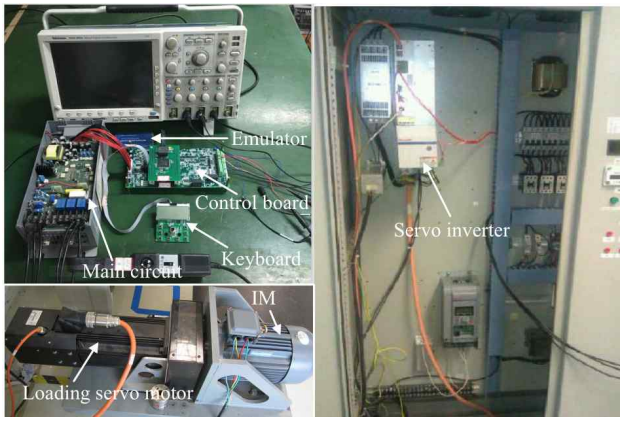

Fig. 5. Experimental platform

6. Experimental Results

Fig. 5 shows the experimental setup, in which the drive system hardware is consisted of an induction machine inverter, an induction machine and a loading system. A Texas Instruments TMS320F28335 digital signal processor (DSP) is adopted as the main processor and the loading system is composed of a servo inverter and a servo motor. In addition, the stator voltage and the stator current are measured by voltage sensor and current hall, respectively. The actual rotor speed of the drive system is measured by a photoelectric encoder (1024 imp/r), which is only used for comparison with the estimated speed.

6.1 Experiments verification for speed estimation during different speed operation

Fig. 6 shows the speed comparison based on SMO and ASMO under different speed command. The IM runs at 3 stages, including 900rpm, 300rpm and 1500rpm, respectively. Moreover, the experimental results are presented by calculating the estimation errors between the real rotor speed ω_r and the estimated rotor speed $\hat{\omega}_r$. It can be seen from Fig. 6 that both SMO and ASMO have good tracking performance, and in which the estimation error of ASMO is smaller than SMO. It means that the proposed method can provide better estimation accuracy. Simultaneously, the oscillation of ASMO is also smaller than SMO when the speed command ω_r^* changes. Therefore, it is conclude from Fig. 6 that the proposed ASMO can present better steady and dynamic properties than the conventional SMO.

Fig. 6 shows the estimated speed response based on SMO and ASMO when the IM runs in full speed range, the corresponding waveform in low speed range is shown in Fig. 7, in which the command speed ω_r^* is from 15 rpm to 150 rpm. It indicates that both SMO and ASMO have good tracking performance, and in low speed region, the estimation error of ASMO is also smaller than SMO. Hence, it means that the proposed ASMO can decrease the estimation error compared with SMO. In addition, the

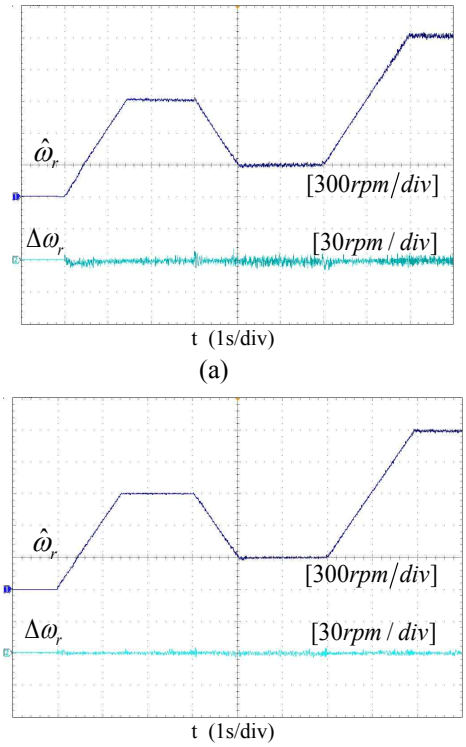

Fig. 6. Experimental results in different speed commands. (a) Speed response based on SMO. (b) Speed response based on ASMO

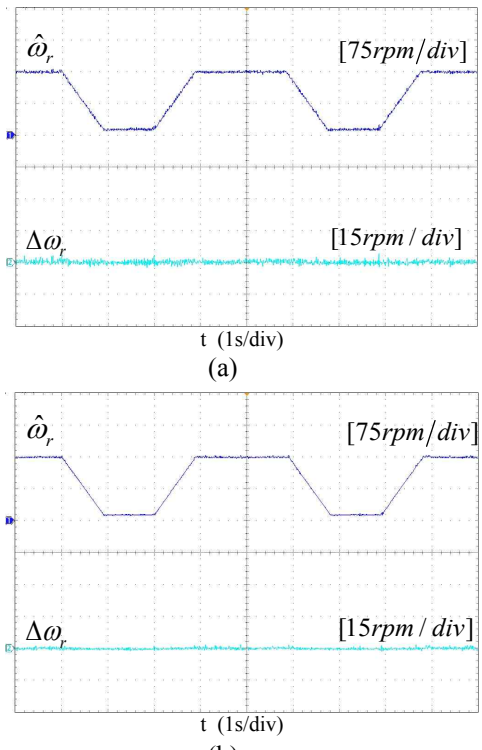

Fig. 7. Experimental results when ω_r^* is from 15 rpm to 150 rpm. (a) Speed response based on SMO. (b) Speed response based on ASMO

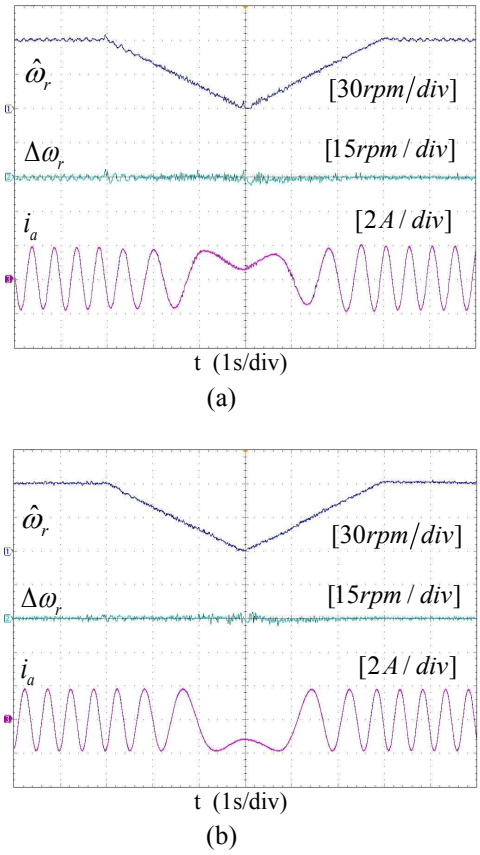

Fig. 8. Experimental results when ω_r^* is from +60rpm to -60rpm. (a) Stator current and speed response based on SMO. (b) Stator current and speed response based on ASMO

oscillation of ASMO is smaller than SMO when ω_r^* changes. Therefore, it can be seen from Fig. 7 that the proposed ASMO can present better properties both in steady state and in transient state.

Fig. 8 shows the stator current and rotor speed response based on SMO and ASMO when ω_r^* is from +60 rpm to -60 rpm. It presents that both SMO and ASMO have good tracking performance in low speed region. In the process of IM speed reversal, the stator current waveform based on SMO has a larger oscillation than the stator current waveform based on ASMO. Simultaneously, it is noted from Fig. 8 that the estimated speed based on ASMO is smoother than SMO on the zero-crossing position, in addition, the speed estimation error based on ASMO is also smaller than SMO both in steady state and in transient state. Hence, it can be conclude from Fig. 8 that the proposed ASMO can present better steady and dynamic properties when IM runs from forward to reversal.

6.2 Experiments of speed estimation under load variation and IM parameters change in low speed range

It can be summarized that the proposed ASMO performs

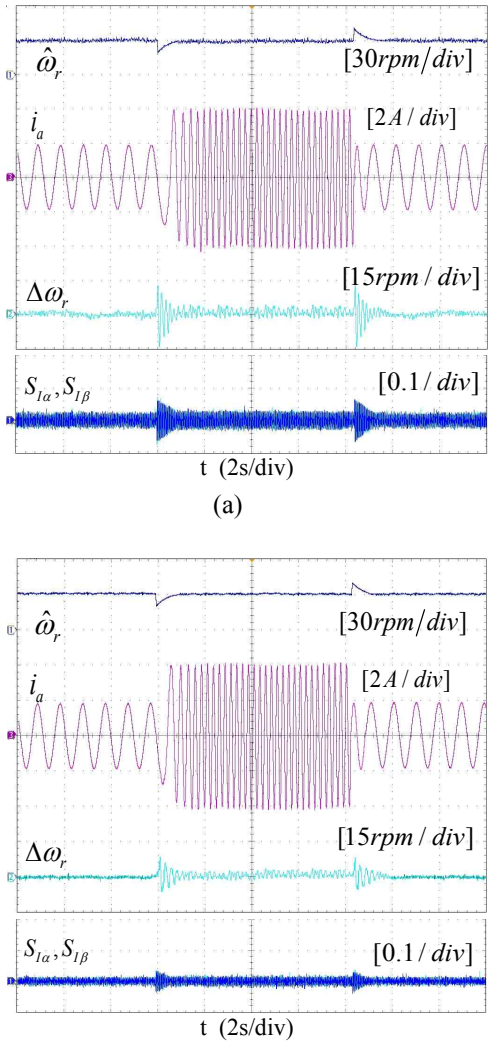

Fig. 9. Experimental results of transient response under step load change in low speed range. (a) SMO. (b) ASMO

better in different speed stage. Moreover, the proposed ASMO also has better performance under load variations. Fig. 9 shows the comparison of stator current, estimated speed, speed estimation error and sliding-mode surface with SMO and ASMO for step load variation in low speed range (30 rpm). The step load steps up from 0 to rated load, and then steps down from rated load to 0. As shown, the speed estimation error of ASMO is smaller than SMO when the step load occurs. In addition, it is known that the sliding-mode surface in SMO is built based on the estimated current error and the rate of the estimated current error, and thus the waveforms of the sliding-mode surface are oscillating near zero since the amplitude of actual stator currents of IM are constantly changing. When the step load occurs, the oscillation of the sliding-mode surface is aggravated because the stator current is changing, and then the estimated current tracks the actual current and the waveforms of the sliding-mode surface keeps stable after

loading. It can be seen from Fig. 9 that both the transient response and the steady accuracy with ASMO are better than the conventional SMO under load variation.

It can be summarized from Fig. 9 that the robustness performance against load disturbance based on the proposed ASMO is better than SMO. Besides, in order to validate the robustness against IM parameters deviation based on the proposed approach, Fig. 10 shows the experimental result with stator resistance deviation $|\Delta R_s|$= 50%. In this experiment, the command speed ω_r^* is set at 30 rpm. When the stator resistance changes by 50%, then larger fluctuations for the estimated speeds occur, in which the largest fluctuations for SMO and ASMO are 11 rpm and 8 rpm, respectively. In addition, for the method of SMO, the oscillations and transitions have occurred into the stator current. However, the stator current based on ASMO keeps smooth. It can be summarized that both two observers can keep stable when the stator resistance changes, however, the robustness of ASMO against stator resistance deviation is stronger.

For testing the robustness against rotor resistance deviation $|\Delta R_r|$=50% in low speed range, Fig. 11 shows the experimental result when the speed command ω_r^* is set at 30 rpm. When the rotor resistance changes by 50%, then larger fluctuations for the estimated speeds occur, in which

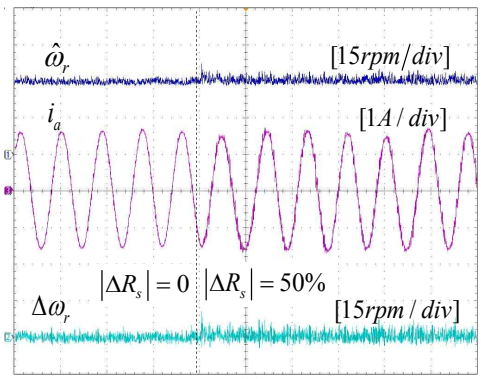

(a)

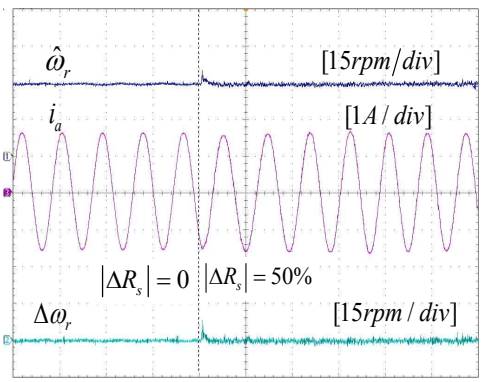

(b)

Fig. 10. Experimental results of robustness against R_s deviation in low speed range. (a) SMO. (b) ASMO

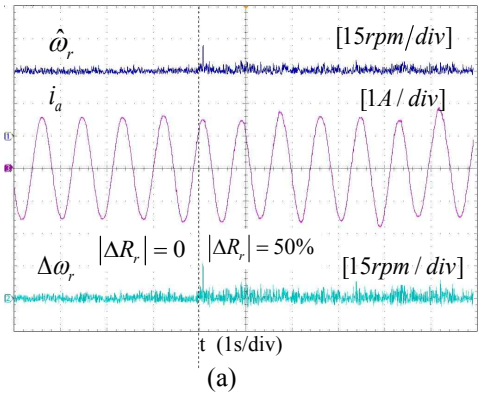

(a)

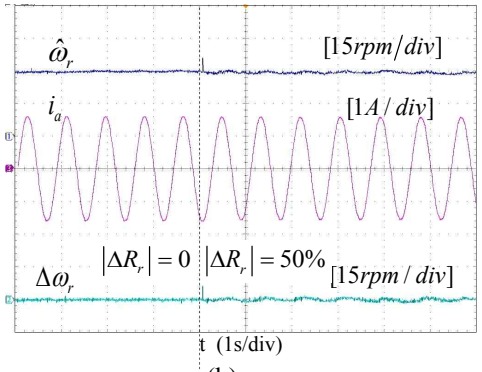

(b)

Fig. 11. Experimental results of robustness against R_r deviation in low speed range. (a) SMO. (b) ASMO

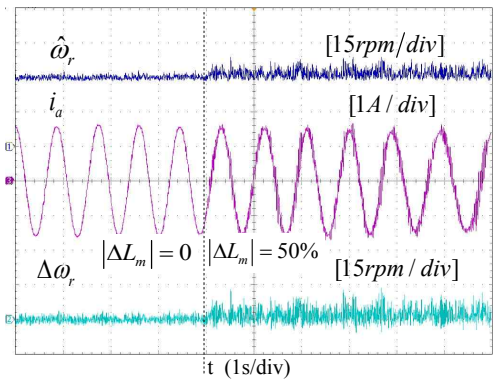

(a)

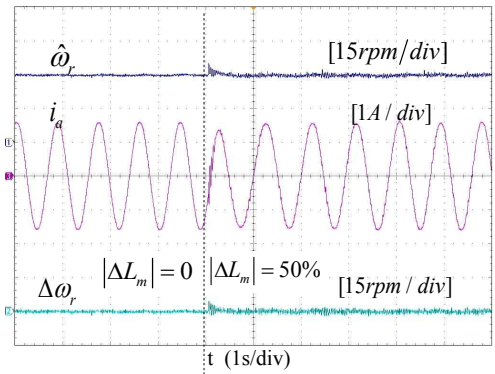

(b)

Fig. 12. Experimental results of robustness against L_m deviation in low speed range. (a) SMO. (b) ASMO

the largest fluctuations for SMO and ASMO are 9 rpm and 6 rpm, respectively. Moreover, the stator current for ASMO has a much smaller fluctuation than SMO because of the optimization algorithm. It is concluded from Fig. 11 that when the rotor resistance changes, both two observers can remain steady, nevertheless, the proposed ASMO is more robust against rotor resistance deviation.

Fig. 12 shows the experimental result with mutual inductance deviation $|\Delta L_m|$=50% when the speed command ω_r^* is set at 30 rpm. When the mutual inductance changes by 50%, then larger fluctuations for the estimated speeds occur, in which the largest fluctuations for SMO and ASMO are 14 rpm and 11 rpm, respectively. In addition, for the method of SMO, the oscillations and transitions have occurred into the stator current. However, the stator current based on ASMO keeps smooth. It is concluded that when the mutual inductance changes, both two observers can keep stable, however, the robustness of ASMO against mutual inductance deviation is stronger.

7. Conclusion

This paper has proposed a novel adaptive sliding-mode observer for speed estimation in sensorless induction machine drives. The proposed method is aiming to balance the dilemma between the requirement of fast reaching transient and the chattering phenomenon reduction which is a well-known problem in sliding-mode observer. By optimizing the reaching way to the sliding-mode surface, an adaptive exponential reaching law is introduced when designing the sliding-mode observer. The adaptive exponential reaching law is based on the options of an exponential term that adapts to the variations of the sliding-mode surface and system states, and the dynamic performance of the adaptive exponential reaching law is analyzed in details. Moreover, the SMO considering the adaptive exponential reaching law, which is called adaptive sliding-mode observer (ASMO), is capable for suppressing the chattering phenomenon and decreasing the reaching time simultaneously. The stability analysis for ASMO is achieved based on Lyapunov stability theory. Simulation and experimental results both demonstrate the validity of the proposed approach.

Appendices

A.1 Stability analysis for adaptive sliding-mode observer based on Lyapunov stability theory

In this paper, the Lyapunov function is selected as follows

$$V = \frac{1}{2} S_I^T S_I \tag{A-1}$$

From (A-1), it is easy to know that Lyapunov function V is positive definite. Then $\dot{V}$ becomes

$$\begin{aligned} \dot{V} &= S_I^T \dot{S}_I \\ &= \begin{bmatrix} S_{I\alpha} & S_{I\beta} \end{bmatrix} \left\{ -g(\tilde{i}_s) \begin{bmatrix} sign(S_{I\alpha}) \\ sign(S_{I\beta}) \end{bmatrix} - \mu \begin{bmatrix} S_{I\alpha} \\ S_{I\beta} \end{bmatrix} \right\} \\ &= -g(\tilde{i}_s) \left[S_{I\alpha} \cdot sign(S_{I\alpha}) + S_{I\beta} \cdot sign(S_{I\beta}) \right] \\ &\quad - \mu \left[S_{I\alpha} \cdot S_{I\alpha} + S_{I\beta} \cdot S_{I\beta} \right] \end{aligned} \tag{A-2}$$

It is easy to know that $S_{I\alpha} \cdot sign(S_{I\alpha}) + S_{I\beta} sign(S_{I\beta}) > 0$ and $S_{I\alpha} \cdot S_{I\alpha} + S_{I\beta} \cdot S_{I\beta} > 0$. Based on (19) and (A-2), it can be concluded that $\mu > 0$ and $0 < g(\tilde{i}_s) < k'/\varepsilon$, then $\dot{V} < 0$ can be satisfied, i.e. the derivative of the Lyapunov function V is negative definite, which means that the observer is asymptotically stable based on Lyapunov stability theory.

Nomenclature

i_s, u_s	Stator current and stator voltage
ψ_s, ψ_r	Stator and rotor flux
R_s, R_r	Stator and rotor resistance
ω_r, ω_{sl}	Rotor speed and slip speed
ω_s (=ω_r +ω_{sl})	Angular rotor flux speed
L_s, L_r, L_m	Stator, rotor and mutual inductances
σ (=1-(L_m^2/L_sL_r))	Leakage coefficient
*	Denotes commanded values
^	Denotes estimated values
~	Denotes the error between estimated values and the actual values
[ ]$_\alpha$, [ ]$_\beta$	Suffixes denoting quantities on stationary reference frame

References

[1] Z. Yin, Y. Zhang, C. Du, J. Liu, X. Sun and Y. Zhong, "Research on anti-error performance of speed and flux estimation for induction motors based on robust adaptive state observer," *IEEE Trans. Ind. Electron*., vol. 63, no. 6, pp. 3499-3510, Jun. 2016.

[2] Y. Zhang, J. Zhu, Z. Zhao, W. Xu and D. G. Dorrell, "An improved direct torque control for three-level inverter-fed induction motor sensorless drive," *IEEE Trans. Power Electron*., vol. 27, no. 3, pp. 1502-1513, Mar. 2016.

[3] K. Wang, B. Chen, G. Shen, W. Yao, K. Lee and Z. Lu, "Online updating of rotor time constant based on combined voltage and current mode flux observer for speed-sensorless AC drives," *IEEE Trans. Ind. Electron*., vol. 61, no. 9, pp. 4583-4593, Sep. 2014.

[4] G. Wang, L. Yang, G. Zhang, X. Zhang and D. Xu,

"Comparative investigation of pseudo-random high frequency signal injection schemes for sensorless IPMSM drives," *IEEE Trans. Power Electron*., vol. 32, no. 3, pp. 2123-2132, Mar. 2017.

[5] W. Sun, J. Gao, Y. Yu, G. Wang and D. Xu, "Robustness improvement of speed estimation in speed-sensorless induction motor drives," *IEEE Trans. Ind. Appl*., vol. 52, no. 3, pp. 2525-2536, May/Jun. 2016.

[6] A. Angelo, M. Cirrincione, M. Pucci and G. Vitale, "Closed-loop MRAS speed observer for linear induction motor drives," *IEEE Trans. Ind. Appl*., vol. 51, no. 3, pp. 2279-2290, May/Jun. 2015.

[7] A. V. R. Teja, V. Verma and C. Chakraborty, "A new formulation of reactive-power-based model reference adaptive system for sensorless induction motor drive," *IEEE Trans. Ind. Electron*., vol. 62, no. 11, pp. 6797-6807, Nov. 2015.

[8] B. Wang, Y. Zhao, Y. Yu, G. Wang, D. Xu and Z. Dong, "Speed-sensorless induction machine control in the field-weakening region using discrete speed-adaptive full-order observer," *IEEE Trans. Power Electron*., vol. 31, no. 8, pp. 5759-5773, Aug. 2016.

[9] W. Sun, Y. Yu, G. Wang, B. Li and D. Xu, "Design method of adaptive full order observer with or without estimated flux error in speed estimation algorithm," *IEEE Trans. Power. Electron*., vol. 31, no. 3, pp. 2609-2626, Mar. 2016.

[10] I. M. Alsofyani and N. R. N. Idris, "Simple flux regulation for improving state estimation at very low and zero speed of a speed sensorless direct torque control of an induction motor", *IEEE Trans. Power Electron*., vol. 31, no. 4, pp. 3027-3035, Apr. 2016.

[11] Z. Yin, C. Zhao, J. Liu, and Y. Zhong, "Research on anti-error performance of speed and flux estimator for induction motor using robust reduced-order EKF," *IEEE Trans. Ind. Informatics*., vol. 9, no. 2, pp. 1037-1046, May. 2013.

[12] Z. Yin C. Zhao, Y. Zhong and J. Liu, "Research on robust performance of speed-sensorless vector control for the induction motor using an interfacing multiple-model extended Kalman filter," IEEE Trans. Power Electron., vol. 29, no. 6, pp. 3011-3019, Jun. 2014.

[13] S. A. Davari, D. A. Khaburi, F. Wang and R. M. Kennel, "Using full order and reduced order observers for robust sensorless predictive torque control of induction motors," *IEEE Trans. Power Electron*., vol. 27, no. 7, pp. 3424-3433, Jul. 2012.

[14] F. Wang, Z. Zhang, S. A. Davari, R. Fotouhi, D. A. Khaburi and J. Rodríguez and R. Kennel, "An encoderless predictive torque control for an induction machine with a revised prediction model and EFOSMO," *IEEE Trans. Ind. Electron*., vol. 61, no. 12, pp. 6635-6644, Dec. 2014.

[15] Z. Yan, C. Jin and V. Utkin, "Sensorless sliding-mode control of induction motors," *IEEE Trans. Ind. Electron*., vol. 47, no. 6, pp. 1286-1297, Dec. 2000.

[16] J. Chen and J. Huang, "Online decoupled stator and rotor resistances adaptation for speed sensorless induction motor drives by a time-division approach," *IEEE Trans. Power Electron*., vol. 32, no. 6, pp. 4587-4599, Jun. 2017.

[17] A. Derdiyok, M. K. Güven, H.-u. Rehman, N. Inanc and L. Xu, "Design and implementation of a new sliding-mode observer for speed-sensorless control of induction machine," *IEEE Trans. Ind. Electron*., vol. 49, no. 5, pp. 1177-1182, Oct. 2002.

[18] A. Derdiyok, "Simple method for speed and rotor resistance estimation of induction machines," *IEE Proc. - Electr. Power Appl*., vol. 150, no. 3, pp. 289-294, May 2003.

[19] H. Rehman, A. Derdiyok, M. K. Güven, L. Xu, "A new current model flux observer for wide speed range sensorless control of an induction machine," *IEEE Trans. Power Electron*., vol. 17, no. 6, pp. 1041-1048, Nov. 2003.

[20] A. Derdiyok, "Speed-sensorless control of induction motor using a continuous control approach of sliding-mode and flux observer," *IEEE Trans. Ind. Electron*., vol. 52, no. 4, pp. 1170-1176, Aug. 2005.

[21] J. Li, L. Xu and Z. Zhang, "An adaptive sliding-mode observer for induction motor sensorless speed control," *IEEE Trans. Ind. Appl*., vol. 41, no. 4, pp. 1039-1046, Jul./Aug. 2005.

[22] Z. Zhang, H. Xu, L. Xu and L. E. Heilman, "Sensorless direct field-oriented control of three-phase induction motors based on 'sliding mode' for washing-machine drive applications," *IEEE Trans. Ind. Appl*., vol. 42, no. 3, pp. 694-701, May/Jun. 2006.

[23] M. Comanescu, "Design and implementation of a highly robust sensorless sliding mode observer for the flux magnitude of the induction motor," *IEEE Trans. Energy Convers*., vol. 31, no. 2, pp. 649-657, Jun. 2016.

[24] Y.-H. Chang, C.-I. Wu, H.-C. Chen, C.-W. Chang and H.-W. Lin, "Fractional-order integral sliding-mode flux observer for sensorless vector-controlled induction motors," *in Proc. American Control Conference* (*ACC*), *San Francisco, USA, 2011*, vol. 3, pp. 190-195.

[25] Y.-H. Chang, C.-I. Wu, H.-W. Lin, H.-C. Chen and C.-W. Chang "Fractional order integral sliding-mode flux observer for direct field-oriented induction machines," *International Journal of Innovative Computing Information and Control*, vol. 8, no. 7(A), pp. 4851-4868, Jul. 2012.

[26] Z. Kandoussi, Z. Boulghasoul, A. Elbacha and A. Tajer, "Fuzzy sliding mode observer based sensorless indirect FOC for IM drives," *in Proc. Third World Conference on Complex Systems (WCCS)*, *Marrakech, Morocco, 2015*, pp. 1-6.

[27] R. P. Vieira, C. C. Gastaldini, R. Z. Azzolin, H. A.

Grundling, "Discrete-time sliding mode speed observer for sensorless control of induction motor drives," *IET Electr. Power Appl.*, vol. 6, no. 9, pp. 681-688, 2012.

[28] A. Mezouar, M. K. Fellah, S. Hadjeri and Y. Sahali "Adaptive speed sensorless vector control of induction motor using singularly perturbed sliding mode observer," *in Proc. IEEE IECON*, 2006, pp. 932-939.

[29] G. Wang, Z. Li, G. Zhang, Y. Yu and D. Xu, "Quadrature PLL-based high-order sliding mode observer for IPMSM sensorless control with online MTPA control strategy," *IEEE Trans. Energy Convers.*, vol. 28, no. 1, pp. 214-224, Mar. 2013.

[30] W. C. A. Pereira, C. M. R. Oliveira, M. P. Santana, T. E. P. d. Almeida, A. G. d. Castro, G. T. Paula and M. L. Aguiar, "Improved sensorless vector control of induction motor using sliding mode observer," *IEEE Latin America Transactions*, vol. 14, no. 7, pp. 3110-3116, Jul. 2016.

Yanqing Zhang was born in Shaanxi, China, in 1989. He received the B.S. and M.S. degrees in Electrical Engineering from Xi'an University of Technology, Xi'an, China, in 2012 and 2015 respectively. He is currently a Ph.D. student in Electrical Engineering, Xi'an University of Technology. His main field of interest is high-performance control of ac motor.

Zhonggang Yin was born in Shandong, China, in 1982. He received the B.S., M.S. and Ph.D. degrees in electrical engineering from Xi'an University of Technology, Shaanxi, China, in 2003, 2006 and 2009, respectively. In 2009, he joined electrical engineering department of Xi'an University of Technology, where he is currently a professor. His research interests include high-performance control of ac motor, and digital control of power converters.

Jing Liu was born in Anhui, China, in 1982. She received the B.S., M.S. and Ph.D. degrees in electronic engineering from Xi'an University of Technology, Shaanxi, China, in 2003, 2006 and 2009, respectively. In 2009, she joined electronic engineering department of Xi'an University of Technology, where she is currently an associate professor. Her research interests include the power semiconductor devices and their application to power electronic devices.

Xiangqian Tong was born in Shaanxi, China, in 1961. He received his B.S. degree in Electrical Engineering from Shaanxi Institute of Technology, Hanzhong, China, and the M.S. degree from Xi'an University of Technology, Xi'an, China, in 1983 and 1989, respectively, and the Ph.D. degree in Electrical Engineering from Xi'an Jiaotong University, Xi'an, in 2006. He joined the Xi'an University of Technology in 1989. Since 2002, he has been a Professor and the Academic Leader of Electrical Engineering with the Xi'an University of Technology. His current research interests include the application of power electronics in power system and control of power quality, especially the power filter, static synchronous compensator, and high voltage direct current.